Computer Simulations of Charge Transport in Dye-Sensitized Nanocrystalline Photovoltaic Cells

Akira Usami*,†,‡ and Hajime Ozaki‡

Department of Electrical, Electronics, and Computer Engineering, Waseda University, 3-4-1 Okubo, Shinjuku-ku, Tokyo 169-8555, Japan, and Central Research Institute of Electric Power Industry, 2-11-1 Iwatokita, Komae-shi, Tokyo 201-8511, Japan

Received: October 6, 2000; In Final Form: January 8, 2001

Charge transport in dye-sensitized nanocrystalline TiO_2 electrodes was studied by a theoretical model. For studies of recombination processes through trap states, a Shockley−Read model, which represents electron transfer through an effective trap level, was used as a recombination term in the model. The simulation results have demonstrated that thermal release of the electrons trapped in shallow tail states to the conduction band contributes to effective electron diffusion in the nanocrystalline electrodes. However, the electrons captured in the tail states at the lowest energy may recombine with oxidized ions in electrolytes. Short-range screening of externally applied biases in the nanocrystalline electrodes was taken into account as a boundary condition in the model. Calculations of current−voltage characteristics have indicated that relatively high open-circuit voltages can be attained under the boundary condition.

1. Introduction

Regenerative photoelectrochemical solar cells based on dye-sensitization of nanocrystalline TiO_2 films have attracted considerable interest as a potential high-efficiency, long-term stable, and low-cost alternative to conventional solid-state solar cells. Grätzel and co-workers have attained energy conversion efficiencies as high as 10−11%.[1−4] However energy conversion efficiencies in almost all verifications[5−8] are much smaller than these high efficiencies. Furthermore recent progress of the highest efficiency is extremely slow. One reason for these is that a definite understanding to energy conversion mechanisms in the photoelectrochemical cells is lacking.

A great number of experiments have contributed to understanding the mechanisms in the photoelectrochemical solar cells. However side reactions in experiments often blind essential features. In theoretical simulations, the basic functioning can be studied by getting rid of the side reactions. Another advantage of theoretical simulations is that one can easily vary values of parameters related to the functioning of solar cells. This is very useful to systematic understanding of the energy conversion mechanisms. Thus it is of great importance to study the energy conversion processes with theoretical models, allowing better understanding of the basic features of the solar cells. However, in contrast to many experiments, few computer simulations of the photoelectrochemical solar cells have been reported.[9−13] In this paper, the authors have studied the energy conversion processes in the sensitized TiO_2 nanocrystalline electrodes with a theoretical model.[9,10,14] Specifically, charge transport influenced by trap states in the nanocrystalline electrodes was simulated using a computer. It should be noted that the object of this paper is not to simulate exactly the real solar cells but to demonstrate the usefulness of computer simulations and illustrate the basic functioning of the nanocrystalline electrodes.

The focus is on the influence of trap states in the dye-sensitized nanocrystalline TiO_2 electrodes. The trap states on TiO_2 nanoparticles are ascribed to defects and disorders of the crystal lattice on the surfaces. The defects are Ti^{4+} atoms in incompletely coordinated lattice and are located at 0.5−0.8 eV below the conduction band edge.[15−17] The disorders are shallow tail states below the conduction band edge.[18] Recent studies have revealed that trapping and detrapping electron processes have great influences on current yields in the nanocrystalline electrodes.[19−23] Furthermore, it has been reported that replacement of adsorbates on the defects by stronger Lewis bases remarkably improves open-circuit voltages.[2,24] Thus these trap states have great influences on both short-circuit currents and open-circuit voltages. In this paper, the authors have simulated the trapping/detrapping processes under short-circuit conditions. An important factor to attain high open-circuit voltages was also studied.

2. Formulation of Theoretical Model

The model first presented for charge transport in TiO_2 nanocrystalline films has consisted of a simple diffusion equation for electrons.[25] However ion transport in electrolytes, which is important to recombination processes, was disregarded in that model. The authors[9,10,14] and a team of Ferber, Stangl, and Luther[11] have proposed simulation models in which the ion transport as well as the electron transport is considered. A difference between our model and the model by Ferber et al. is as follows: a Shockley−Read model[26] is a recombination term in our model, whereas a simple first-order model is the term in the model by Ferber et al. The Shockley−Read recombination model which represents electron transfer through an effective

* Corresponding author. E-mail: usami@criepi.denken.or.jp.
† Department of Electrical, Electronics, and Computer Engineering, Waseda University.
‡ Central Research Institute of Electric Power Industry.

10.1021/jp0036801 CCC: $20.00
Published on Web 04/27/2001

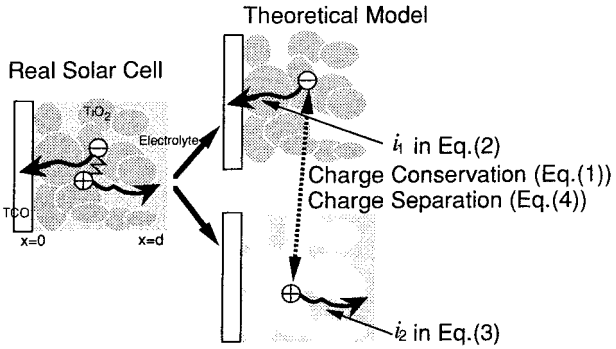

Figure 1. Schematic images of the dye-sensitized nanocrystalline solar cells and the modeling of the solar cells.

trap level permits studies on the influences of the trap states. This is an advantage of our model because the intricate charge transport processes due to the trap states[20−23,27] are essential for the simulations.

In terms of the theoretical simulations of the trap effects, Nelson's work applying a continuous-time random-walk model (CTRW)[12] should be cited. An absolute difference between the CTRW and our model is the simulation method. Our model is an analytical simulation model solving equations, whereas the CTRW is a Monte Carlo simulation model following traces of electrons.

2.1. Basic Equations. Schematic images of the model for the charge transport are shown in Figure 1. We adopt an assumption in battery theories[28,29] to the modeling for the nanocrystalline electrodes. Specifically, without going into the geometric detail of the nanocrystalline electrode, the porous material is treated as a superposition of two continua. That is, one represents a pore-filling solution and the other a solid semiconductor matrix. Current i_1 and i_2 are introduced for the electrons in the matrix and the ions in the solution, respectively. Total current is obtained as the sum of i_1 and i_2.

The model is represented as the following in one-dimensional form:

$$\frac{\mathrm{d}i_1}{\mathrm{d}x} + \frac{\mathrm{d}i_2}{\mathrm{d}x} = 0 \tag{1}$$

$$i_1 = \epsilon\mu_\mathrm{n} n \frac{\mathrm{d}\epsilon_\mathrm{F}}{\mathrm{d}x} \tag{2}$$

$$i_2 = \frac{2\epsilon(\mu_3 - 3\mu_1)}{2 + \ln\gamma} C_3 \frac{\mathrm{d}\mu}{\mathrm{d}x} \tag{3}$$

$$\frac{\mathrm{d}i_1}{\mathrm{d}x} = -\mathrm{e}\Phi\alpha\exp(-\alpha x) + \mathrm{e}\frac{2nC_3}{2\tau_{\mathrm{n}0}C_3 + \tau_{\mathrm{CO}}(n + n_\mathrm{i}\exp(-\epsilon_\mathrm{t}/k_\mathrm{B}T))} \tag{4}$$

Here n,ϵ_F, C_3, and μ without the subscript are electron density in the semiconductor matrix, quasi-Fermi level in the semiconductor matrix, triiodide ion concentrations in the solution, and chemical potential of the ions, respectively. μ with the subscript is mobility. The subscripts of n, 1, and 3 in the mobilities represent electron, iodide ion, and triiodide ion, respectively. γ is the activity coefficient of the ions, e is elementary charge, ϵ is correction factor, α is absorption coefficient for incident light by dye-sensitizers, Φ is intensity of incident photons, τ_{no} is electron lifetime, τ_{co} is ion lifetime, n_i is effective density of states in the TiO_2 conduction band, κ_B is the Boltzmann constant, T is absolute temperature, and ϵ_t is an effective single energy level of the traps below the conduction band edge.

The first equation represents charge conservation; divergence of the total current is zero. The second and third equations are current equations for the electrons and ions, respectively. The correction factor ϵ represents decrease in the mobilities due to nanocrystalization. In eq 3, from net chemical reactions in the electrolyte $I_3^- + 2e^- \leftrightarrows 3I^-$, the following is assumed: $\mathrm{d}C_1{:}-\mathrm{d}C_3 = 3{:}1$, denoting iodide ion concentration by C_1. In the last equation, the light absorption and the recombination are described. In the light absorption term, which is the first term on the right-hand side, the solar cell is illuminated from the interface between the nanocrystalline electrode and the transparent conductive oxide (TCO) electrode ($x = 0$). The light absorption term represents current yields due to electron injections into the semiconductor matrix. The second term on the right-hand side is the Shockley−Read recombination model which represents current losses due to electron transfer from the semiconductor matrix to the electrolyte through the trap states. The electron lifetime τ_{no} is related to the electron trapping kinetics in the semiconductor matrix. The ion lifetime τ_{co} is related to the recombination kinetics between the trapped electrons and the oxidized ions. In this model, recombination of the injected electrons with the oxidized state of the dye-sensitiers is omitted owing to its fast reduction by the iodide ions in the electrolyte.[4] In the recombination model, electron transfer from the reduced ions to the trap states is also omitted. The effective trap energy level ϵ_t represents the distributed energy levels as an effective energy level, and its origin is at the conduction band edge. The details of the formulation are described in ref 14 as well.

2.2. Boundary Conditions. In addition to eqs 1−4, four boundary conditions must be considered. The three boundary conditions among these are the following: $i_1(d) = 0$, $i_2(0) = 0$, and $i_1(0) = i_2(d)$, where d is the nanocrystalline TiO_2 electrode thickness. In the last condition, it is assumed that an applied external voltage changes the electron density at $x = 0$; the change depends on the Fermi−Dirac distribution.

In the model, we assume that an externally applied voltage is completely neutralized at the boundary between the sensitized nanocrystalline film and the TCO electrode ($x = 0$). That is, the intrinsic Fermi level drops to the redox level within a region so thin as to be negligible. This assumption is based on the following screening effect: ion motion in the electrolyte neutralizes the applied bias over a short range in the nanocrystalline electrode.[30] Strictly speaking, this boundary model is valid under the upper limits of the ion concentrations over the electron density in the semiconductor matrix. This is consistent with the fact that the concentrations of the ions are generally 2 orders of magnitude greater than the electron density. Therefore field-driven drift terms are omitted in the numerical computation although the terms are implicit in eqs 2 and 3.

2.3. Recombination Model. The recombination models of the reduction processes of the oxidized ions are classified into first-order models and second-order models. In the second-order models, electron acceptors in the electrolytes are I_2 molecules, while these are $I^\bullet$ radicals in the first-order models.[23] Recent studies have indicated that the recombination is not a first-order process but a second-order process.[23,31] As concentrations of $I^\bullet$ and I_2 under $C_1 \gg C_3$ are proportional to $C_3^{1/2}$ and C_3, respectively, the Shockley−Read model is a second-order model

TABLE 1: Parameters of the Theoretical Model

symbols	values used in calculations	notes
λ	650 nm	wavelength of incident light
$\alpha(\lambda)$	1.95×10^5 m^{-1}	absorption coefficient of electrode
D_s^*	5.0×10^{-5} cm^2 s^{-1}	diffusion coefficient of electrons in semiconductor matrix
$D_{I^-}^*$, $D_{I_3^-}^*$	2.6×10^{-6} cm^2 s^{-1}	diffusion coefficients of iodide and triiodide in electrolyte pores
d	10 μm	nanocrystalline electrode thickness
I_o	100 mW cm^{-2}	incident light intensity
τ_{no}	10 ms	electron lifetime under short-circuit
n_i	3.1×10^{21} cm^{-3}	effective density of states of conduction band

in terms of the electron acceptor species because we should substitute $C_3^{1/2}$ for C_3 in the recombination term of a first-order process.

On the other hand, in terms of form, the Shockley−Read recombination model agrees with a first-order model n/τ_{no} when trap filling and the electron detrapping are ignored ($\tau_{no}C_3 \gg \tau_{co}(n + n_i \exp(-\epsilon_t/\kappa_B T))$). For the correction, the decrease of the electron lifetime described in ref 10 is taken into account when an external voltage is applied. This is because the first-order model is coincident with a second-order model if the lifetime in the first-order model is in inverse proportion to the electron density. In fact, the lifetime in the first-order recombination decreases as the electron density in the semiconductor matrix increases.[23,32]

2.4. Numerical Computation Method. The numerical computation of the nonlinear differential equations is divided into two parts.[14] In the first part, discretization of the currents in space is conducted by following calculations in the PC-1D program[33] except for the field-driven drift terms. Unfortunately, resultant equations cannot be solved easily because of derivatives from the nonlinear term in the recombination. In the second part, the nonlinear equations are solved using the Newton−Raphson method.[34] A great advantage of the procedure is that simulations can be carried out by personal computers. The details of the method are presented in the Appendix and ref 14.

3. Estimations of Values of Parameters

The theoretical model permits studies of the recombination processes influenced by the trap sites. Unfortunately, definite values of those parameters are not known. Thus, reasonable values to illustrate and highlight the basic features and functioning of the nanostructured electrodes were used. These values are listed in Table 1.

One can estimate light absorption coefficient α and electron diffusion length $(D_s^*\tau_{no})^{0.5}$ from incident photon-to-current conversion efficiency (IPCE) and wavelength dependence of light absorption by the dye molecules.[10] The electron diffusion coefficient D_s^* includes the correction factor ϵ. Shift in the light absorption due to the adsorption of the dye sensitizers onto the TiO_2 can be ignored because the shift is relatively small. The resultant typical diffusion lengths were 7−9 μm.[10] To estimate each value of the electron diffusion coefficient D_s^* and the electron lifetime τ_{no}, either of these must be available. According to the battery theories,[28,29] the electron diffusion coefficient D_s^* is calculated from the porosity and the electron diffusion coefficient in the crystal of 0.02 cm^2 s^{-1}.[35] However the resultant value was much greater than experimental values.[22,36] The difference between the estimation and experiments is ascribed to electron hopping on the surfaces and charge compensation by ion clouds in the electrolytes.[22,36] Thus the electron diffusion coefficient D_s^* is close to diffusion coefficients of the ions in the electrolytes. The listed values of the electron diffusion coefficient D_s^* and the electron lifetime τ_{no} were estimated from the above discussion and a review of literature.[37]

The diffusion coefficients of the ions in the electrolytes are available from the literature.[38] $D_{I^-}/D_{I_3^-}$ is 1.0−1.3. Measured diffusion coefficients of triiodide vary greatly with solvents: in acetonitrile, $> 8.5 \times 10^{-6}$ cm^2 s^{-1} ; in 3-methyl-2-oxazolidinone (NMO), 2.8×10^{-6} cm^2 s^{-1}. The values in Table 1 were considering porosity as well. The light intensity was set to be the same as solar irradiation under fine weather. However it should be noted that the incident light is monochromatic in the model. The effective density of states in the conduction band is available from ref 39. The film thickness is a typical value in ref 2. A 100% light reflectance at the Pt counter electrode mirror[2] was also assumed. In all calculations, concentrations of the triiodide ions in the dark are 50 ± 0.1 mM.

The remaining parameter in these estimations is the ion lifetime τ_{co}. This parameter is related to electron-transfer time from the trap states to the ions in the electrolyte. If K_1 and τ' are defined in the second-order models as follows[23,24,31]

$$I_3^- \overset{K_1[M]}{\rightleftharpoons} I_2 + I^- \tag{5}$$

$$I_2 + e \xrightarrow{\tau'[s]} \frac{1}{2}(I_3^- + I^-) \tag{6}$$

the ion lifetime τ_{co} becomes $(C_1/K_1)\tau'$. As C_1 and K_1 are about 10^{-1} M and 10^{-7} M, respectively, the ion lifetime τ_{co} is about 6 orders of magnitude greater than τ'. However the ion lifetime τ_{co} cannot be estimated from τ' because the value of τ' is not known. Thus we have inferred the value of the ion lifetime τ_{co} from the following rough estimations. First of all, it is boldly assumed that the ion lifetime τ_{co} is 10^{-1} s. Under this assumption, both $\tau_{co}n$ and $\tau_{no}C_3$ become about 10^{23} sm^{-3} in I_o = 100 mW cm^{-2} because n and C_3 are about 10^{18} cm^{-3} and 10^1 mM, respectively. Then, the simplest recombination term $nC_3/(\tau_{co}n + \tau_{no}C_3)$ is used for the estimations. From the above result, a substitution of $\tau_{co}n$ for $\tau_{no}C_3$ and an omission of 2 in the resultant denominator make the recombination term n/τ_{no}. Furthermore, as the difference between the values of the electron lifetime τ_{no} and the first assumed ion lifetime τ_{co} is only 1 order of magnitude, a second assumption is $\tau_{no} = \tau_{co}$. Under these assumptions, the electron-transfer kinetics from the semiconductor matrix to the electrolyte is represented as the following equation: $dn/dt = -n/\tau_{co}$, denoting time by t. Thus the electron-transfer time is 10^{-1} s under the assumptions owing to the solution $n \propto \exp(-t/\tau_{co})$. This value agrees with the experimental time scale of the electron transfer from the semiconductor matrix to the electrolyte.[40] This agreement suggests that the ion lifetime τ_{co} is the order of the time scale of the electron transfer or of the electron lifetime τ_{no} because of the first and second assumptions

4. Results and Discussion

4.1. Trapping/Detrapping Processes on TiO_2 Surfaces. In the first calculations, we focused on the thermal detrapping processes of the electrons trapped in the surface states under short-circuit conditions. Dependence of the recombination current on the effective trap energy level ϵ_t is shown in Figure 2. In the calculations, $\tau_{no} = \tau_{co}$ was assumed. This figure reveals that the recombination current through the trap states becomes

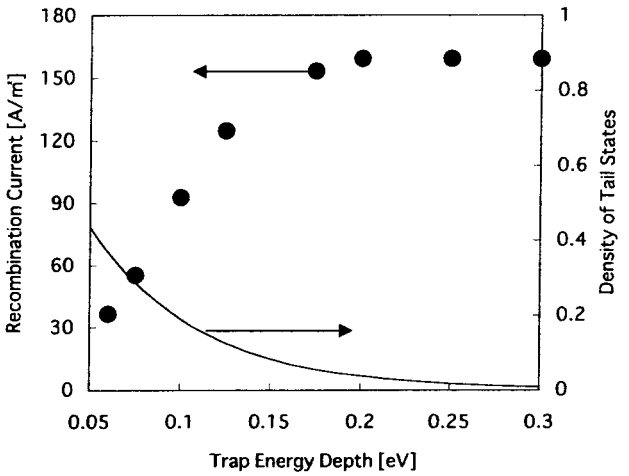

Figure 2. Dependence of the recombination current on the effective energy level of the trap states. The trap energy depth is measured from the conduction band edge. In the calculations, $\tau_{no} = \tau_{co}$ was assumed. The density distribution of the tail states normalized by the density at the conduction band edge is shown. The slope of the distribution is 60 meV.

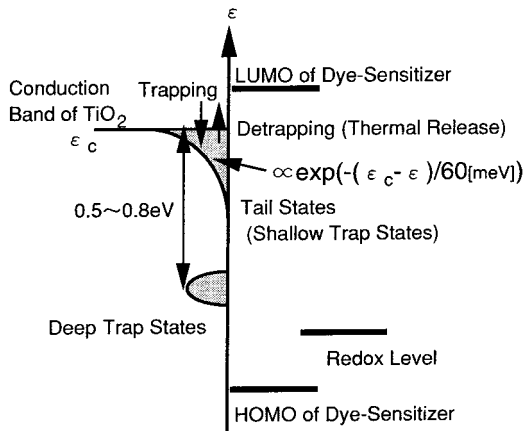

Figure 3. Schematic image of the dye-sensitized TiO_2 nanoparticle surfaces. The equation represents the density distribution of the tail states. ϵ_c is the energy level at the conduction band edge.

less and less as the effective trap energy level ϵ_t gets closer to the conduction band edge. This is due to the thermal release of the trapped electrons. A schematic image of the real trap states is depicted in Figure 3. The energy levels of the Ti^{4+} atoms are about 0.5−0.8 eV below the conduction band edge.[15−17] Thus the calculation results reveal that the energy levels of the Ti^{4+} atoms are too deep to release the trapped electrons to the conduction band. The other trap states are distributed exponentially with a slope of about 60 meV below the conduction band edge.[23,27] When the effective trap energy level ϵ_t of this tail state is 60 meV below the conduction band edge, the recombination current is much smaller than the saturated recombination current at deeper energy levels in Figure 2. This indicates that the majority of the electrons trapped in the shallow tail states can diffuse in the nanocrystalline electrode to the TCO electrode without the recombination because of the thermal release.

Recent studies have revealed that the trapping/detrapping processes through the shallow tail states have great influences on the functioning of the solar cells.[19−23] A recombination model has been presented;[21] there is a demarcation energy level ${}_nE_d$ that defines whether the recombination with the oxidized ions in the electrolyte or the thermal release to the conduction band

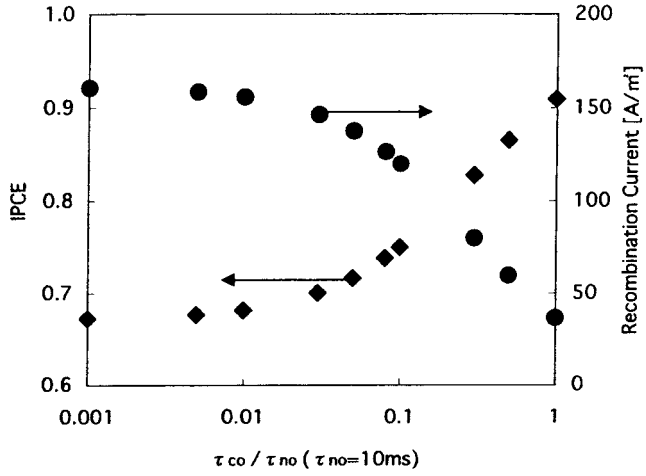

Figure 4. Dependence of the IPCE and the recombination current on the ion lifetime τ_{co}. IPCE is incident photon-to-current conversion efficiency. The effective trap energy level is 60 meV below the conduction band edge.

is the dominant relaxation process of the trapped electrons. It has been also reported that the energy level ${}_nE_d$ is located between the energy levels of the tail states and Ti^{4+} atoms.[21] In other words, the electrons trapped in the tail states do not reduce the oxidized ions owing to the thermal release. Thus this model is in agreement with the simulation results.

In the above calculations, the ion lifetime τ_{co} has the same value as the electron lifetime τ_{no}. However the ion lifetime τ_{co} may conceivably be overestimated because a definite value of ion lifetime τ_{co} is unknown. For a confirmation of the above discussion, dependence of the recombination current on the ion lifetime τ_{co} was calculated. The results are depicted in Figure 4. The effective trap energy level ϵ_t was set to be 60 meV below the conduction band edge in the calculations. This figure indicates that the thermal release cannot improve the current yields if the ion lifetime τ_{co} is 2 orders of magnitude smaller than the electron lifetime τ_{no}. However the ion lifetime τ_{co} is probably not so small on the basis of the rough estimations. Thus, these calculations also corroborate the above discussion.

However it should be noted that the lowest part in the energy distribution of the tail states overlaps the energy levels where the recombination currents are saturated as shown in Figure 2. This indicates that the demarcation energy level ${}_nE_d$ may get into the tail states. Thus the above discussion strongly depends on the energy distribution of the tail states. In fact, the recombination current is not small enough to be negligible even under the condition that the recombination current through the Ti^{4+} atoms is probably small. [41−43]

4.2. Current−Voltage Characteristics. In the above subsection, it is indicated that the energy levels where the trapped electrons are scarcely released to the conduction band become the recombination centers. The recombination current decreases not only the short-circuit current but also the open-circuit voltage. The theoretical model permits studies under externally applied biases. Thus the open-circuit voltage is discussed in this subsection.

First of all, the dependence of the IPCE on the ion lifetime τ_{co} was calculated again to confirm the existence of the recombination current. The results are shown in Figure 5. The detrapping processes are omitted in the calculations. These results reveal that several seconds in τ_{co} are required to completely prevent the recombination current. As already mentioned, a definite value of the ion lifetime τ_{co} is unknown.

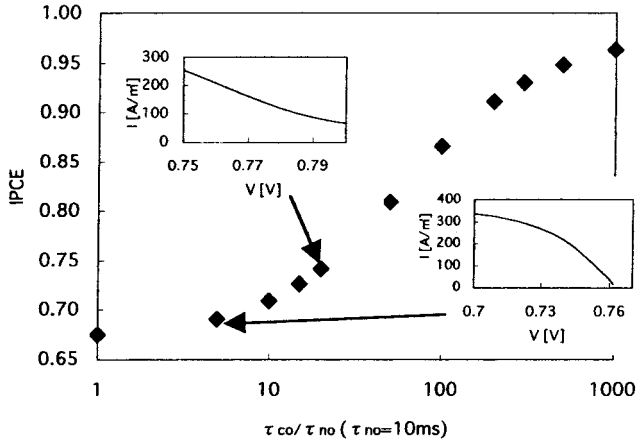

Figure 5. $I-V$ characteristics and IPCE dependence on the ion lifetime τ_{co}. The inserted graphs are $I-V$ characteristics when the ion lifetime τ_{co} is 50 and 200 ms. In the $I-V$ characteristics, I and V are the current and the externally applied voltage, respectively. Energy difference between the conduction band edge and the redox level is assumed to be 0.95 eV from ref 4. The thermal release is omitted in the calculations. In other words, the effect is included, if any, in the diffusion coefficient of electrons in the semiconductor matrix. IPCE is incident photon-to-current conversion efficiency.

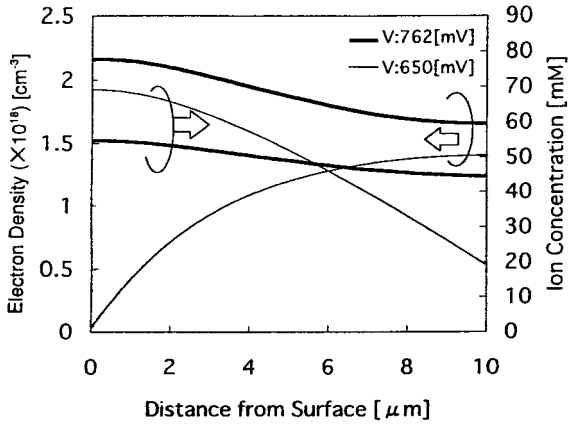

Figure 6. Charge distributions in the nanocrystalline electrodes. $d = 10\ \mu$m, and $\tau_{co} = 50$ ms. The voltages of 650 and 762 mV are close with those under the highest electric power and the open-circuit, respectively.

However the order of seconds in τ_{co} is probably too great on the basis of the rough estimations. Thus, the existence of the recombination current is reasonable.

The results of the $I-V$ characteristics simulations under $\tau_{co} = 50$ ms and $\tau_{co} = 200$ ms [10] are inserted in Figure 5. These indicate that relatively high open-circuit voltage V_{oc} can be attained owing to the diffusion process in the electrodes. However open-circuit voltages of the real solar cells[1−8] are smaller than the resultant voltages. One reason for the potentially high V_{oc} can be discussed using the charge distributions in the nanocrystalline electrodes. The charge distributions at voltages of 650 and 762 mV under $\tau_{co} = 50$ ms are shown in Figure 6. The distributions of the electrons and ions under the low bias indicate that both currents i_1 and i_2 are attributed to the gradients of the respective concentrations. Under the high bias, both the charge concentrations become smaller as the distance from the surface becomes farther away. This reveals that the potentially high V_{oc} is ascribed to accumulation of the electrons in the vicinity of the TCO electrode. The screening effect under the boundary condition is a cause of this. Needless to say, we cannot conclude on all vital factors for the voltages from this discussion because many factors have influences on the potential distributions in the nanocrystalline electrodes.[44] The operation in the part adjacent to the TCO electrode has been controversial still.[45,46] Furthermore the reduction of the oxidized dyes by the electrons, which is omitted in the simulations, depends on the externally applied voltage.[47,48] This also might be responsible for the lower V_{oc}. Nevertheless this discussion has proposed that improvement of the recombination in the vicinity of the TCO electrode is important for high efficiency.

5. Conclusion

In this paper, the usefulness of computer simulations by theoretical models was demonstrated. The electron transport in the dye-sensitized nanocrystalline electrodes was studied using the theoretical model. The results have demonstrated the importance of thermal release of the electrons trapped in the shallow tail states for effective electron transport. The $I-V$ characteristics calculations have indicated that the relatively high open-circuit voltages are potentially attained. For the high open-circuit voltages, the charge transport in the part close to the TCO electrodes in the dye-sensitized nanocrystalline films is an important factor. Unfortunately the studies by the theoretical model were restricted to a qualitative discussion rather than a quantitative discussion. Nevertheless, we believe that theoretical studies contribute to the understanding of the basic functioning of the nanocrystalline photovoltaic cells.

Appendix

The method of solving numerically the four nonlinear differential equations in the model is described here. The procedure is divided into two parts. In the first part, the four differential equations become four series of nondifferential equations at discrete points in x. Unfortunately, these equations cannot easily be solved yet because of the nonlinear equations derived from eq 4. In the second part, the nonlinear equations are solved using the Newton−Raphson method.

We followed the discretization in the PC-1D program for the discretization in eq 2. However it should be noted that the intrinsic Fermi level is constant in space because we have omitted the field-driven drift. In the method, the current and quasi-Fermi level are not spatially uniform within an element but given a linear spatial variation within an element. Then eq 2 at node k becomes

$$i_1(x_k^+) = -\frac{\Delta x_k}{\Delta \xi_k}\left[\frac{di_1}{dx}\right]_k [1 - Z(\Delta \xi_k)] + \frac{D_s^*}{\Delta x_k}\eta_{k+1}\Delta \xi_k Z(\Delta \xi_k) \quad \text{(A1)}$$

where Δx_k is $x_{k+1} - x_k$, $\Delta \xi_k$ is $\epsilon_{F,k+1}/k_BT - \epsilon_{F,k}/k_BT$, D_s^* is the electron diffusion coefficient, and η_k is en_k. The expression is simplified by making use of the Bernoulli function: $Z(y) = y/(\exp(y) - 1)$. $i_1(x_k^+)$ is calculated between node k and $k+1$. The current at node k can be calculated between node k and $k-1$. The equation is

$$i_1(x_k^-) = -\frac{\Delta x_{k-1}}{\Delta \xi_{k-1}}\left[\frac{di_1}{dx}\right]_{k-1} [1 - Z(-\Delta \xi_{k-1})] + \frac{D_s^*}{\Delta x_{k-1}}\eta_k \Delta \xi_{k-1} Z(\Delta \xi_{k-1}) \quad \text{(A2)}$$

where this current is denoted by $i_1(x_k^-)$. Using eqs A1 and A2, the current equation for the electrons at node k becomes

$$i_1(x_k^+) = i_1(x_k^-) \tag{A3}$$

It should be noted that $i_1(x_k^-)$ and $i_1(x_k^+)$ do not exist at $x = 0$ ($k = 0$) and $x = d$ ($k = N$), respectively. The current equation for the ions at node k becomes an expression similar to eq A3, assuming that the activity coefficient γ is spatially uniform within an element.

Discretization in eq 4 gives di_1/dx at node k and $k - 1$ in eqs A1 and A2:

$$\left[\frac{di_1}{dx}\right]_k \Delta x_k = e\Phi[e^{-\alpha x_{k+1}} - e^{-\alpha x_k}] + \frac{(\eta_{k+1} + \eta_k)(\chi_{k+1} + \chi_k)}{2\tau_{n0}(\chi_{k+1} + \chi_k) + \tau_{c0}\left(\eta_{k+1} + \eta_k + 2\eta_i \exp\left(-\frac{\epsilon_t}{\kappa_B T}\right)\right)} \Delta x_k \tag{A4}$$

Here χ_k represents FC_3 at node k if a unit of C_3 is mol and the Faraday constant is denoted by F. di_2/dx at node k and $k - 1$ is also derived from eq A4, using the following equation from eq 1:

$$\left[\frac{di_2}{dx}\right]_k \Delta x_k = -\left[\frac{di_1}{dx}\right]_k \Delta x_k \tag{A5}$$

The boundary equations are

$$\mu_1 - \mu_0 = \left[\frac{d\mu}{dx}\right]_0 \Delta x_0 \tag{A6}$$

$$\epsilon_{F,N} - \epsilon_{F,N-1} = \left[\frac{d\epsilon_F}{dx}\right]_{N-1} \Delta x_{N-1} \tag{A7}$$

$$i_1(0^+) = i_2(d^-) \tag{A8}$$

$$n(0) = n_i \exp\left(-\frac{\epsilon_c - \epsilon_{red/ox} - V}{\kappa_B T}\right) \tag{A9}$$

where ϵ_c, $\epsilon_{red/ox}$, and V are energy levels of conduction band edge and redox couples and externally applied voltage, respectively. In eqs A6 and A7, both $[d\mu/dx]_0$ and $[d\epsilon_F/dx]_{N-1}$ are zero.

In the second part, a Jacobian matrix for the Newton−Raphson method is generated using the analytical derivatives of each equation in terms of the quasi-Fermi level and the chemical potential of the ions. First of all, an approximate solution is required. The solutions to the simple diffusion equations for the electrons and the ions were adopted as the approximation to the electron density and the ion concentration, respectively. Specifically, for example, the equation for the electrons is

$$D_s^* \frac{d^2 n}{dx^2} - \frac{n - n_0}{\tau} + \Phi\alpha e^{-\alpha x} = 0 \tag{A10}$$

The solution is

$$n(x) = n_0 + \frac{1}{2}\left\{(n(0) - n_0) - \sqrt{\tau D_s^*}\frac{dn}{dx_{x=0}} - \frac{\alpha\tau\Phi}{1 - \sqrt{\tau D_s^*}\alpha}\right\} e^{-x/(\tau D_s^*)^{1/2}} + \frac{1}{2}\left\{(n(0) - n_0) + \sqrt{\tau D_s^*}\frac{dn}{dx_{x=0}} - \frac{\alpha\tau\Phi}{1 + \sqrt{\tau D_s^*}\alpha}\right\} e^{x/(\tau D_s^*)^{1/2}} + \frac{\alpha\tau\Phi}{1 - \tau D_s^* \alpha^2} e^{-\alpha x} \tag{A11}$$

without the light reflection at the counter electrode.

References and Notes

(1) O'Regan, B.; Grätzel, M. *Nature (London)* **1991,** *353*, 737.

(2) Nazeeruddin, M.K.; Kay, A.; Rodicio, I.; Humphry-Baker, R.; Müller, E.; Liska, P.; Vlachopoulos, N.; Grätzel, M. *J. Am. Chem. Soc.* **1993,** *115*, 6382.

(3) Barbe, C. J.; Arendse, F.; Comte, P.; Jirousek, M.; Lenzmann, F.; Shklover, V.; Grätzel, M. *J. Am. Ceram. Soc.* **1997,** *80*, 3157.

(4) Hagfeldt, A.; Grätzel, M. *Chem. Rev.* **1995**, *95*, 49.

(5) Knödler, R.; Sopka, J.; Harbach, F.; Grünling, H.W. *Sol. Energy Mater. Sol. Cells* **1993**, *30*, 277.

(6) Smestad, G.; Bignozzi, C.; Argazzi, R. *Sol. Energy Mater. Sol. Cells* **1994,** *32*, 259.

(7) Hagfeldt, A.; Didriksson, B.; Palmqvist, T.; Lindström, H.; Södergren, S.; Rensmo, H.; Lindquist, S.-E. *Sol. Energy Mater. Sol. Cells* **1994,** *31*, 481.

(8) Matthews, D.; Kay, A.; Grätzel, M. *Aust. J. Chem.* **1994**, *47*, 1869.

(9) Usami, A. *Jpn. J. Appl. Phys.* **1997**, *36*, L886.

(10) Usami, A. *Chem. Phys. Lett.* **1998**, *292*, 223.

(11) Ferber, J.; Stangl, R.; Luther, J. *Sol. Energy Mater. Sol. Cells* **1998**, *53*, 29; Stangl, R.; Ferber, J.; Luther, J. *Sol. Energy Mater. Sol. Cells* **1998,** *54*, 255.

(12) Nelson, J. *Phys. Rev.* **1999,** *B59*, 15374.

(13) There is some theoretical work using a much simple model and focusing on one property of the solar cells; for example, on the electron injections: Matthews, D.; Infelta, P.; Grätzel, M. *Sol. Energy Mater. Sol. Cells* **1996,** *44*, 119. On the ion diffusion processes: ref 38 in this paper. On light scattering in the nanocrystalline films: Usami, A. *Sol. Energy Mater. Sol. Cells* **2000,** *62*, 239 and references therein.

(14) Usami, A. *Proc. IEEE Photovoltaic Spec. Conf.* **2000,** *28*, in press.

(15) Redmond, G.; Fitzmaurice, D.; Grätzel, M. *J. Phys. Chem.* **1993,** *97*, 6951.

(16) Boschloo, G.K.; Goossens, A. *J. Phys. Chem.* **1996,** *100*, 19489.

(17) Boschloo, G.; Fitzmaurice, D. *J. Phys. Chem.* **1999**, *B103*, 2228.

(18) Kay, A.; H.-Baker, R.; Grätzel, M. *J. Phys. Chem.* **1994,** *98*, 952.

(19) Schwarzburg, K.; Willig, F. *Appl. Phys. Lett.* **1991,** *58*, 2520.

(20) Cao, F.; Oskam, G.; Meyer, G. J.; Searson, P. C. *J. Phys. Chem.* **1996,** *100*, 17021.

(21) Franco, G.; Gehring, J.; Peter, L. M.; Ponomarev, E. A.; Uhlendorf, I. *J. Phys. Chem.* **1999**, *B103*, 692.

(22) Solbrand, A.; Henningsson, A.; Södergren, S.; Lindström, H.; Hagfeldt, A.; Lindquist, S.-E. *J. Phys. Chem.* **1999**, *B103*, 1078.

(23) Fisher, A. C.; Peter, L. M.; Ponomarev, E. A.; Walker, A. B.; Wijayantha, K. G. U. *J. Phys. Chem.* **2000**, *B104*, 949.

(24) Huang, S.Y.; Schlichthörl, G.; Nozik, A.J.; Grätzel, M.; Frank, A.J. *J. Phys. Chem.* **1997**, *B101*, 2576.

(25) Södergren, S.; Hagfeldt, A.; Olsson, J.; Lindquist, S.-E. *J. Phys. Chem.* **1994**, *98*, 5552.

(26) Shockley, W.; Read, W. T., Jr. *Phys. Rev.* **1952**, *87*, 835.

(27) van de Lagemaat, J.; Frank, A. J. *J. Phys. Chem.* **2000**, *B104*, 4292.

(28) Newman, J.; Tiedemann, W. *AIChE J.* **1975**, *21*, 25.

(29) Gu, H.; Nguyen, T. V.; White, R. E. *J. Electrochem. Soc.* **1987**, *134*, 2953.

(30) Zaban, A.; Meier, A.; Gregg, B.A. *J. Phys. Chem.* **1997,** *B101*, 7985.

(31) Schlichthörl, G.; Huang, S. Y.; Sprague, J.; Frank, A. J. *J. Phys. Chem.* **1997,** *B101*, 8141.

(32) Könenkamp, R.; Henninger, R. *Appl. Phys.* **1994,** *A58*, 87.

(33) Rover, D.T.; Basore, P.A.; Thorson, G.M. *Proc. IEEE Photovoltaic Spec. Conf.* **1985,** *18,* 703.

(34) Press: W. H.; Teukolsky, S. A.; Vetterling, W. T.; Flannery, B. P. *Numerical Recipes in C*, 2nd ed.; Cambridge University Press: Cambridge, U.K., 1992; p 379.

(35) O'Regan, B.; Moser, J.; Anderson, M.; Grätzel, M. *J. Phys. Chem.* **1990,** *94*, 8720.

(36) Solbrand, A.; Lindström, H.; Rensmo, H.; Hagfeldt, A.; Lindquist, S.-E.; Södergren, S. *J. Phys. Chem.* **1997,** *B101*, 2514.

(37) Hagfeldt, A. *Sol. Energy Mater. Sol. Cells* **1995,** *38* , 339.

(38) Papageorgiou, N.; Grätzel, M.; Infelta, P. P. *Sol. Energy Mater. Sol. Cells* **1996,** *44* , 405.

(39) Heimer, T. A.; Bignozzi, C. A.; Meyer, G. J. *J. Phys. Chem.* **1993,** *97*, 11987.

(40) Salafsky, J. S.; Lubberhuizen, W. H.; van Faassen, E.; Schropp, R. E. I. *J. Phys. Chem.* **1998,** *B102*, 766.

(41) This is due to the estimated diffusion lengths shorter than the electrode thicknesses.[10] The small recombination current through the Ti^{4+} atoms was estimated from dependence of the short-circuit current on pyridine treatment in the nanocrystalline electrode. Specifically, the pyridine treatment has little influence on the short-circuit current of the cell used for the diffusion length estimation,[2] although a majority of the deeper trap states

vanishes by the pyridine treatment (ref 15 and Moser et al.; loc. cit.). On the other hand, it should be noted that the influence strongly depends on conditions in the sensitized nanocrystalline electrodes (refs 2, 24, and Lindström et al.; loc. cit.).

(42) Moser, J.; Punchihewa, S.; Infelta, P. P.; Grätzel, M. *Langmuir* **1991,** *7*, 3012.

(43) Lindström, H.; Rensmo, H.; Södergren, S.; Solbrand, A.; Lindquist, S.-E. *J. Phys. Chem.* **1996,** *100*, 3084.

(44) Cahen, D.; Hodes, G.; Grätzel, M.; Guillemoles, J.F.; Riess, I. *J. Phys. Chem. B* **2000,** *104*, 2053.

(45) Schwarzburg, K.; Willig, F. *J. Phys. Chem.* **1999**, *B103*, 5743.

(46) Pichot, F.; Gregg, B. A. *J. Phys. Chem.* **2000,** *B104*, 6.

(47) Haque, S. A.; Tachibana, Y.; Klug, D. R.; Durrant, J. R. *J. Phys. Chem.* **1998,** *B102*, 1745.

(48) Haque, S. A.; Tachibana, Y.; Willis, R. L.; Moser, J. E.; Grätzel, M.; Klug, D. R.; Durrant, J. R. *J. Phys. Chem.* **2000,** *B104*, 538.